Controllable helical collapse caused by a nonlinearity-related Gouy phase shift

Dan Wang,[1,*] Xin Zhang,[1] Rui-Wei Li,[1] Fan Feng,[1] Lin Lu,[2] Hui Feng,[2]
Biao Feng,[3] Shao-Ding Liu,[1] and Zhong-Quan Nie[4,†]

[1]*Key Lab of Advanced Transducers and Intelligent Control System, Ministry of Education and Shanxi Province, College of Electronic Information and Optical Engineering, Taiyuan University of Technology, Taiyuan 030024, China*

[2]*College of Physics, Taiyuan University of Technology, Taiyuan 030024, China*

[3]*College of Electrical and Power Engineering, Taiyuan University of Technology, Taiyuan 030024, China*

[4]*College of Advanced Interdisciplinary Studies, National University of Defense Technology, Changsha 410073, China*

(Received 4 May 2024; accepted 12 August 2024; published 30 August 2024)

Helical filamentation of optical fields has gained significant attention due to its potential physical properties, complexity, and practicality. However, conventional methods of manipulating filament formation face a major challenge in achieving controllable helical filamentation. We propose a method to manipulate helical collapse based on a nonlinearity-related Gouy phase shift. This method is triggered by the nonlinear interaction between vector vortex beams and anisotropic Kerr media. It is uncovered that, in the absence of the vortex, the radially polarized beam can only form the multifilament at specific locations in a BaF_2 crystal. Nevertheless, once the vortex is attached, the beam can rotate based on the multifilament. The direction and angle of the rotation can be controlled by varying the topological charge number of the vortex phase. In addition, spin-orbit coupling and a rotational nonlinear refractive phase shift are generated during the helical collapse process. Finally, the physical mechanism behind this helical collapse is illustrated by a nonlinearity-related Gouy phase shift. This research presents a different approach to controlling optical field collapse and filamentation, with potential applications in various fields, including optical communications, optical manipulation, and optical microprocessing.

DOI: 10.1103/PhysRevA.110.023529

I. INTRODUCTION

With the wide application of femtosecond laser filamentation, helical filamentation has received more and more attention due to the special propagation trajectory [1–3]. However, it remains a significant challenge to achieve controllable rotation while precisely controlling the number and position of the collapsed filaments. On the one hand, the collapse and filamentation of the optical field become random due to the Kerr induction modulation instability caused by random noise [4–12]. On the other hand, achieving optical field controllable rotation during collapse filamentation is also a major difficulty, which will show novel properties and unique applications in many applications of filament formation.

Conventional methods of controlling optical filamentation mainly involve manipulating the spatial structure of the scalar optical field in both phase and amplitude [13–18]. In recent years, vector optical fields have also been used to investigate controllable optical field collapse and filament formation due to their unique polarization properties. Controllable and stable collapse of various vector optical fields into filaments in isotropic and anisotropic Kerr media have been achieved by manipulating the polarization state distribution of the optical field [19–24]. Yet, one limitation of these methods is their inability to achieve controllable rotation in the collapse position during collapse filamentation. In this regard, the vortex beam is a good candidate for this purpose. It can indeed rotate in the direction dictated by the chirality of this vortex during collapse filamentation [25–27], but it is difficult to control the position and number of collapse filaments. In conclusion, the controllable helical filamentation of optical fields remains an area for further investigation.

Inspired by the above challenge, this work presents a method for achieving controllable helical collapse of vector vortex beams in anisotropic Kerr media. Furthermore, we discover a nonlinearity-related Gouy phase shift caused by the nonlinear interaction of the optical field with the medium. It is revealed that in the absence of the vortex, the radially polarized beam can only form the multifilament at certain locations in a BaF_2 crystal. Once the vortex is present, however, the beam can rotate on the basis of the multifilament. During this helical collapse, the nonlinear interaction between the beam and the medium will result in spin-orbit coupling and a rotational nonlinear refractive phase shift. The rotation of nonlinear refractive phase shift distribution affects the phase distribution of the optical field, generating a nonlinearity-related Gouy phase shift that leads to helical collapse. Moreover, the direction and angle of the rotation are determined by the orbital angular momentum carried by the incident field, which can be modulated by changing the topological charge of the vortex phase. Lastly, a possible experimental prototype is proposed preliminarily. This method opens up a way for controllable optical field collapse

*Contact author: wangdan@tyut.edu.cn
†Contact author: niezhongquan@tyut.edu.cn

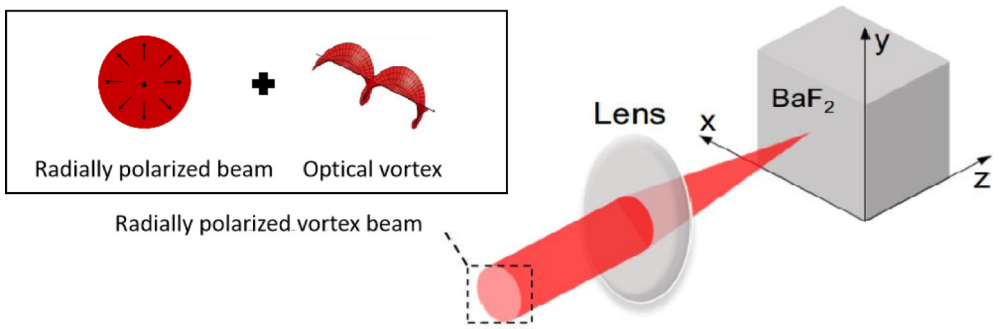

FIG. 1. The nonlinear propagation schematic of the radially polarized vortex beam in a BaF_2 crystal. A radially polarized vortex beam is focused by a focusing lens and propagates along the [001] crystal axis of a thick BaF_2 crystal. The red beam represents a radially polarized vortex beam, and the lens represents a focusing lens. The gray square is a thick BaF_2 cubic crystal.

and filamentation, which has enormous application value in many fields such as guided microwave radiation [28], generation of millijoule femtosecond supercontinuum spectral sources [29], optical communications [30], and terahertz radiation enhancement [31].

II. THEORETICAL ANALYSIS

First, this work analyzes the nonlinear propagation behavior of a radially polarized vortex beam in an anisotropic Kerr medium. Under the weak focusing situation, a radially polarized vortex beam can be written as

$$\mathbf{E}_\perp = [E_x\hat{\mathbf{e}}_x + E_y\hat{\mathbf{e}}_y] = A(r)\exp(jm\varphi)(\cos\varphi\hat{\mathbf{e}}_x + \sin\varphi\hat{\mathbf{e}}_y), \tag{1}$$

where $\hat{\mathbf{e}}_x$ and $\hat{\mathbf{e}}_y$ are a pair of orthogonal line polarization unit vectors in the polar coordinate system (r, φ); φ is the azimuth angle; $A(r) = A_0 r\exp(-r^2/2r_0^2)$ and $\exp(jm\varphi)$ represent the spatial distribution of the amplitude and the phase, respectively; m denotes the vortex phase topological charge; and r_0 is the radius of the focal ring. When $m = 0$, the optical field degenerates into a normal radially polarized optical field with a hollow structure and without orbital angular momentum (OAM). When $m \neq 0$, the optical field is a radially polarized vortex optical field with a hollow structure and OAM.

BaF_2 crystal, as an example of anisotropic Kerr media, whose third-order nonlinear polarization intensity strongly depends on the polarization angle of the incident optical field as well as the crystal orientation. In this work, we consider that a vector vortex beam is incident on the BaF_2 crystal and propagates parallel to the [001] crystallographic axis (the z-axis direction in Fig. 1). In order to investigate the nonlinear propagation behavior of the vector vortex beams in this crystal, a $(2+1)$-dimensional vector-version nonlinear Schrödinger (NLS) equation should be used. Under the slowly varying envelope and paraxial approximations, the NLS equation can be divided into a pair of coupled NLS equations for two orthogonal components as follows [21],

$$j\frac{\partial\psi_x}{\partial\zeta} + \nabla_\perp^2\psi_x + \frac{8P}{P_{\rm cr}}|\psi_x|^2\psi_x + \frac{8P}{P_{\rm cr}} \times \left(\frac{1-\sigma}{3}\right)(2|\psi_y|^2\psi_x + (\psi_y)^2\psi_x^*) = 0 \tag{2a}$$

$$j\frac{\partial\psi_y}{\partial\zeta} + \nabla_\perp^2\psi_y + \frac{8P}{P_{\rm cr}}|\psi_y|^2\psi_y + \frac{8P}{P_{\rm cr}} \times \left(\frac{1-\sigma}{3}\right)(2|\psi_x|^2\psi_y + (\psi_x)^2\psi_y^*) = 0, \tag{2b}$$

where $\psi_x(\psi_y)$ is the dimensionless x (y) component normalized by the total field as

$$\psi_{x,y}(\rho,\varphi;\zeta) = \frac{E_{x,y}(\rho,\varphi;\zeta)}{\sqrt{\iint|E_x(\rho,\varphi;\zeta)|^2 + |E_y(\rho,\varphi;\zeta)|^2\rho d\rho d\varphi}}, \tag{3}$$

where $\rho = r/r_0$ and $\zeta = z/4z_d$ are the dimensionless cylindrical coordinates; $z_d = \pi r_0^2/\lambda$ is the Rayleigh distance of the optical field propagating within a vacuum; $P = 2n_0\varepsilon_0 c\iint|E_x(\rho,\varphi;\zeta)|^2 + |E_y(\rho,\varphi;\zeta)|^2\rho d\rho d\varphi$ is the incident power; $P_{\rm cr} = \alpha\lambda^2/4\pi n_0 n_2$ represents the critical powers for self-focusing, where n_2 is the nonlinear refractive index; n_0 denotes the linear refractive index; λ, ε_0, and c are the wavelength, the permittivity, and the speed of light in the free space, respectively; α is a parameter related to a Gaussian profile and so should be taken as $\alpha = 2$ [32]; and σ is the the anisotropy parameter. For the isotropic Kerr media, $\sigma = 0$. For the anisotropic Kerr media, $\sigma \neq 0$, and for a BaF_2 crystal, $\sigma = -1.2$ [33]. On the left-hand side of Eq. (2), the second term represents the contribution from the diffraction described by the transverse Laplacian $\nabla_\perp^2 = \partial^2/\partial\rho^2 + \rho^{-1}\partial/\partial\rho + \rho^{-2}\partial^2/\partial\varphi^2$. The third and fourth terms are from the Kerr nonlinearity. It is evident that Eq. (2) fails to satisfy the principle of linear superposition, and there exists no universal analytical solution. However, we can still simulate the propagation characteristics of the vector vortex beams in anisotropic Kerr media based on the beam propagation method [34]. As is well known, when $m \neq 0$, the optical field is a radially polarized vortex optical field, which will carry the orbital angular momentum induced by the vortex phase [35,36]. Moreover, the orbital angular momentum of the optical field is inextricably linked to the phase distribution of the optical field. Therefore, to facilitate the investigation of the physical mechanisms behind the propagation behavior of the radially polarized vortex beam propagating in a BaF_2 crystal, the optical angular momentum and phase theories are analyzed in this section.

Based on the definition of angular momentum (AM) density, it is apparent that the angular momentum density in the propagation direction can also be divided into two parts: OAM density and spin angular momentum (SAM) density $\mathbf{j}_z = \mathbf{j}_z^o + \mathbf{j}_z^s$. Then j_z^o and j_z^s can be written as [37],

$$j_z^o \propto \mathrm{Im}\left(E_x^* \frac{\partial E_x}{\partial \varphi} + E_y^* \frac{\partial E_y}{\partial \varphi}\right),$$
$$j_z^s \propto \mathrm{Im}(E_x^* E_y - E_x E_y^*). \quad (4)$$

The AM distribution is reflected by the AM density, whereas the average AM in the propagation direction can be expressed as [37–40]

$$J_z = \frac{\iint j_z dxdy}{E} = \frac{\int j_z^o dxdy}{E} + \frac{\int j_z^s dxdy}{E} = J_z^o + J_z^s, \quad (5)$$

where E represents the full energy of the optical field, J_z^o denotes the average OAM, and J_z^s denotes the average SAM.

According to Eq. (1), the transverse optical field $\mathbf{E}_\perp$ can be regarded as a superposition of the x-direction component $\mathbf{E}_x$ and the y-direction component $\mathbf{E}_y$. In this work, we specify the magnitude and the direction of $\mathbf{E}_\perp$ as

$$E_\perp = \sqrt{\left(E_x^2 + E_y^2\right)},$$
$$\psi = \arctan\left(E_y / E_x\right). \quad (6)$$

Therefore, the phase of $\mathbf{E}_i$ can be expressed as $\Delta_i = \arctan[\mathrm{Im}(E_i)/\mathrm{Re}(E_i)]$, $i = x, y$, and $\perp$.

III. RESULTS

According to the principle outlined in Fig. 1, this work numerically simulates the propagation characteristics of the radially polarized vortex beams with different vortex phases propagating along the [001] crystallographic axis in a BaF_2 crystal at an incident power of $P = 6P_{cr}$.

When $m = 0$, the optical field degenerates into an ordinary radially polarized optical field. As the propagation distance increases, the optical field collapses into four filaments at fixed locations, as shown in Fig. 2 (first row). When $m \neq 0$, the optical field is a radially polarized vortex optical field. As the propagation distance increases, the optical field not only collapses into four filaments but also rotates during the collapse process, as shown in Fig. 2 (from the second row to the fifth row). If $m > 0$, the optical field carries a positive vortex and rotates counterclockwise, as shown in Fig. 2 (second and third rows). If $m < 0$, the optical field carries a negative vortex and rotates clockwise, as shown in Fig. 2 (fourth and fifth rows). For $m = \pm 1$, the optical field rotates by 0°, 7°, 14°, and 20° (Corresponding to ζ is 0, 0.05, 0.11, and 0.18 in turn), respectively, as shown in Fig. 2 (second and fourth rows). For $m = \pm 3$, the optical field rotates by 0°, 19°, 34°, and 48° (Corresponding to ζ is 0, 0.07, 0.13, and 0.22 in turn), respectively, as shown in Fig. 2 (third and fifth rows). The rotation angle during the collapse process increases as the propagation distance and the absolute value of m increases. Therefore, the direction and angle of the rotation can be modulated by varying the vortex phase topological charge m. To comprehensively observe the nonlinear propagation characteristics of radially polarized vortex beams in a BaF_2 crystal, this work numerically simulates the propagation in three dimensions for $m = 0$ and $m = \pm 3$, respectively, at the same incident power, as shown in Fig. 3. The propagation behavior illustrated in Fig. 3 is consistent with the results of Fig. 2.

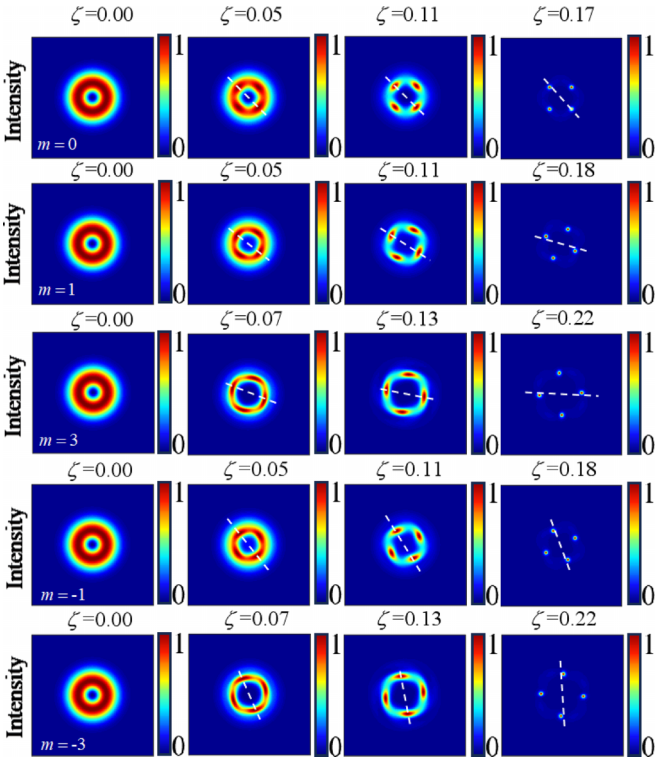

FIG. 2. The intensity of radially polarized vortex beams with different vortex phases propagating in a BaF_2 crystal. The topological charges of the vortex phases are $m = 0$ (first row), $m = \pm 1$ (second and fourth rows), and $m = \pm 3$ (third and fifth rows). Each row from left to right corresponds to four sequentially increasing propagation distances ζ. The white dotted lines reflect the change in rotation angle. The intensity is normalized to its maximum value in each image separately. The color bar represents normalized light intensity values.

The above results show that radially polarized beams without a vortex will collapse into four filaments at fixed locations. However, radially polarized vortex beams will collapse into four filaments and rotate along the vortex chiral direction as it propagates in the BaF_2 crystal. In addition, the rotation angle can be modulated by varying the vortex phase topological charge m. Compared to normal radially polarized beams, radially polarized vortex beams carry OAM induced by the vortex phase. For an optical field with a particular polarization and phase structure, its AM can be divided into OAM and SAM. In general, these two types of angular momentum are independent and conserved in their own way. However, in some anisotropic Kerr media, the conservation of these two angular momenta is lost and the spin-orbit interaction occurs [41,42]. To investigate the role of AM in this helical collapse, the variation curves of OAM and SAM of radially polarized vortex beams with different vortex phases propagating in a BaF_2 crystal are simulated at the same incident power, as shown in Figs. 4 and 5.

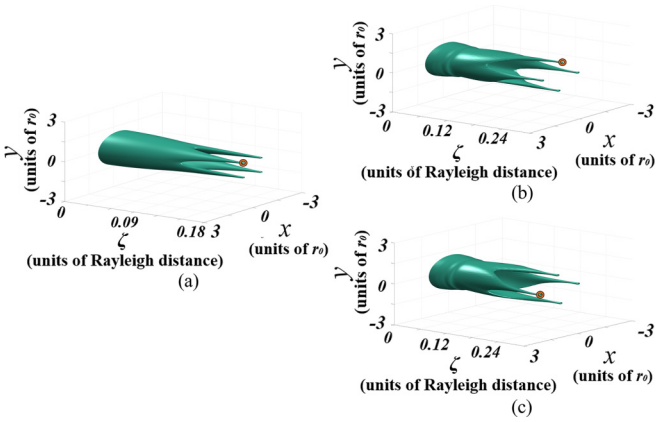

FIG. 3. Three-dimensional collapse diagram of radially polarized vortex beams with different vortex phases propagating in a BaF_2 crystal. The topological charges of the vortex phases are $m = 0$ (a), $m = 3$ (b), and $m = -3$ (c). The orange circle reflects the rotation during the optical field collapse. The units of the x axis and the y axis are r_0. The unit of the propagation distance ζ is the Rayleigh distance.

When $m = 0$, the incident optical field carries no OAM or SAM. The average SAM and the average OAM of the optical field remain conserved as the propagation distance increases, as shown in Figs. 4 and 5. When $m \neq 0$, the incident optical field carries the OAM caused by the vortex phase. As the propagation distance increases, the average OAM and the average SAM of the optical field are no longer conserved, and spin-orbital coupling occurs. Among them, changes in the average OAM are more apparent, as shown in Figs. 4 and 5. When $m > 0$, the optical field carries a positive OAM. As the propagation distance increases, the absolute value of the

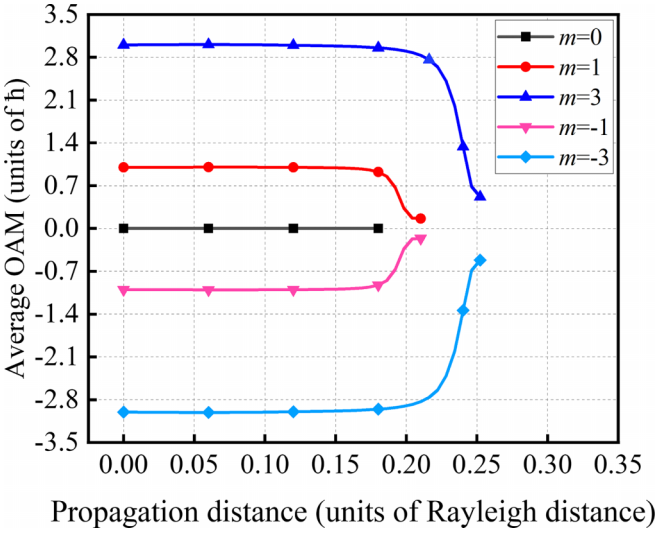

FIG. 4. The average OAM variation curve of radially polarized vortex beams with different vortex phases propagating in a BaF_2 crystal. The topological charges of the vortex phases are $m = 0$ (black with square curve), $m = 1$ (red with circle curve), $m = -1$ (pink with inverted triangle curve), $m = 3$ (blue with triangle curve), and $m = -3$ (light blue with lozenge curve). The unit of the average OAM is $\hbar$.

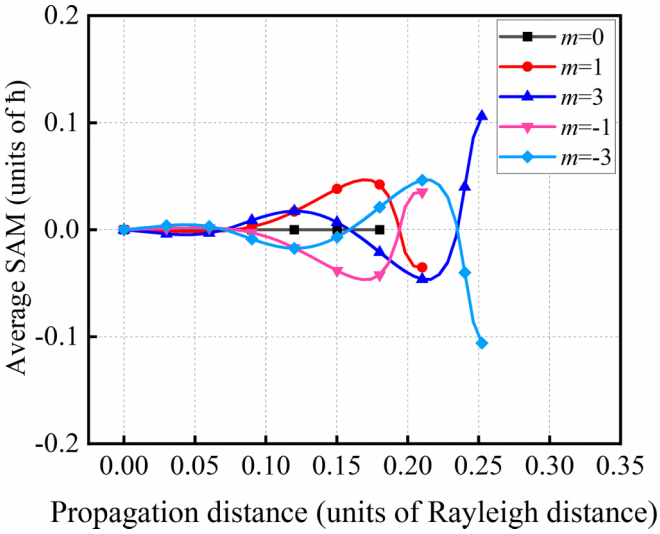

FIG. 5. The average SAM variation curve of radially polarized vortex beams with different vortex phases propagating in a BaF_2 crystal. The topological charges of the vortex phases are $m = 0$ (black with square curve), $m = 1$ (red with circle curve), $m = -1$ (pink with inverted triangle curve), $m = 3$ (blue with triangle curve), and $m = -3$ (light blue with lozenge curve). The unit of the average SAM is $\hbar$.

average OAM decreases. Similarly, when $m < 0$, the optical field carries a negative OAM, and the absolute value of the average OAM decreases with the propagation distance increasing. As the absolute value of m increases, the absolute value of the average OAM of the incident field will also increase. Additionally, the decrease in the absolute value of the average OAM during the collapse will also increase, as shown in Fig. 4. On the other hand, although the average SAM is not conserved, it will only fluctuate slightly with propagation, as shown in Fig. 5. Thus, the average AM exhibits a decreasing trend during the collapse. This reduction in AM may be absorbed by the medium when the optical field interacts with it.

To summarize, in a BaF_2 crystal, the helical collapse of the radially polarized vortex beam is regulated by the OAM carried by the incident field. The rotation direction is determined by the direction of the OAM, and the rotation angle is determined by the magnitude of the OAM. Therefore, we can control the rotation by adjusting the vortex phase topological charge. With the spin-orbit coupling, the conservation of the SAM and the OAM is lost, and the change of the OAM becomes dominant. It is widely acknowledged that the phase of the optical field is closely related to the OAM carried by the optical field. Therefore, it is highly probable that changes in the optical field OAM will be accompanied by changes in the phase distribution. This section will further analyze the phase change of radially polarized vortex beams in a BaF_2 crystal at the same incident power, as shown in Fig. 6.

When $m = 0$, as the propagation distance increases, the phase distribution will gradually concentrate on the four collapsed positions of the optical field, as shown in Fig. 6 (first row). When $m \neq 0$, as the propagation distance increases, the phase distribution not only gradually concentrates on the four

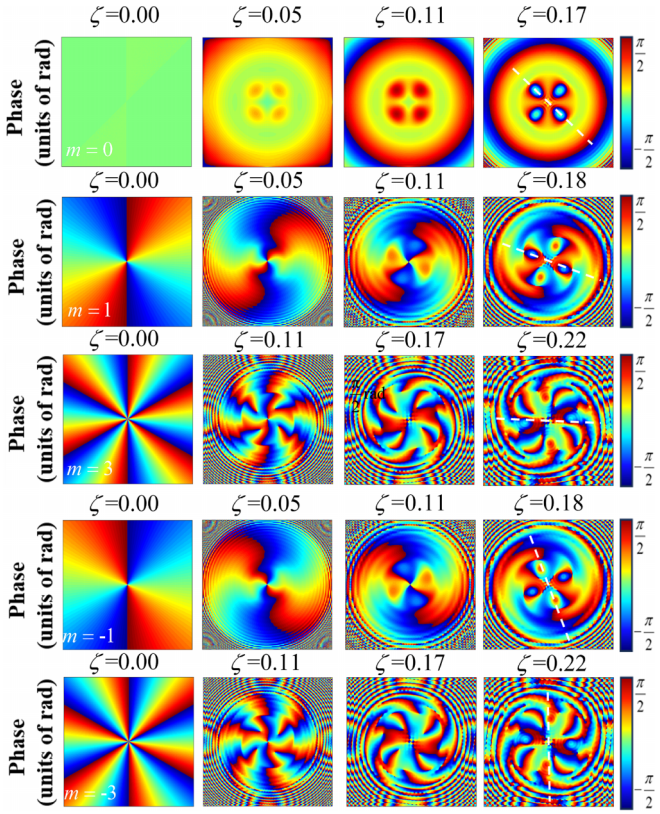

FIG. 6. The phase of radially polarized vortex beams with different vortex phases propagating in a BaF_2 crystal. The topological charges of the vortex phases are $m = 0$ (first row), $m = \pm 1$ (second and fourth rows), and $m = \pm 3$ (third and fifth rows). Each row from left to right corresponds to four sequentially increasing propagation distances ζ. The white dotted lines reflect the change in rotation angle. The color bar represents phase values in radians.

collapsed positions of the optical field but also rotates, as shown in Fig. 6 (from second row to fifth row). If $m > 0$, the optical field phase rotates counterclockwise, as shown in Fig. 6 (second and third rows). If $m < 0$, the optical field phase rotates clockwise, as shown in Fig. 6 (fourth and fifth rows). For $m = \pm 1$, the optical field phase rotates by 20° during the whole collapse process, as shown in Fig. 6 (second and fourth rows). For $m = \pm 3$, the optical field phase rotates by 48° during the whole collapse process, as shown in Fig. 6 (third and fifth rows). The rotation angle during the whole collapse process increases as the propagation distance and the absolute value of m increases.

It is evident that an additional phase shift occurs during the propagation. The rotating phase causes the optical field to rotate almost synchronously with the phase during the collapse. It is similar to the Gouy phase shift that occurs when a focused beam passes through a focal point. The Gouy phase shift of the radially polarized vortex vector optical field described by Eq. (1) during propagation can be expressed as follows [43,44],

$$W(m, \zeta) = (|m| + 1)\arctan(\zeta). \tag{7}$$

According to Eq. (7), the Gouy phase shift of radially polarized vortex beams can be calculated. When the m of the incident beam is ±1, the Gouy phase shift of the beam is 0°, 6.2°, 13°, and 20.4° (correspondingly ζ is 0, 0.05, 0.11, and 0.18 in turn), respectively. When the m of the incident beam is ±3, the Gouy phase shift is 0°, 17°, 31°, and 50° (Correspondingly ζ is 0, 0.07, 0.13, and 0.22 in turn), respectively. Obviously, the angle calculated according to Eq. (7) is consistent with the rotation angle of the intensity and phase in Figs. 2 and 6 (fourth column). Thus, it can be obtained that the radially polarized vortex beam does produce a Gouy phase shift as it propagates in the BaF_2 crystal.

IV. DISCUSSIONS

From the above analytical results, it can be concluded that a radially polarized vortex beam propagating in a BaF_2 crystal will produce a Gouy phase shift that causes the beam to rotate as it collapses. While the conventional Gouy phase shift is generally produced by the beam in different linear focusing systems [45–47]. In contrast, the Gouy phase shift in this work occurs in a nonlinear anisotropic Kerr medium. What is the reason for this special Gouy phase shift? When beams pass through a thin sample of BaF_2 along the [001] crystallographic axis, a nonlinear refractive phase shift is generated due to the nonlinear interaction of the optical field with the medium [48]. The nonlinear refractive phase shift affects the phase of the beam. Is the appearance of the Gouy phase shift related to the nonlinear refractive phase shift? To illustrate the physical mechanism behind this special Gouy phase shift, we consider the nonlinear refractive phase shift produced by a radially polarized vortex beam propagating in a thick BaF_2 crystal. For the specific geometry of BaF_2 crystals, the effective third-order nonlinear refractive index is expressed as [49]

$$n_{\text{eff}}(\theta) = n_2^0[1 + 2\sigma(\sin^4\theta - \sin^2\theta)], \tag{8}$$

where n_2^0 is the third-order nonlinear refraction index related to the real part of the third-order susceptibility tensor $\chi^{(3)}_{1111}$, and θ is the polarization angle of the beam with respect to the [100] crystallographic axis. For a thin sample of BaF_2 crystal, the nonlinear refractive phase shift produced by the beam passing through the crystal along the z axis can be expressed as [48]

$$\delta_0 = k n_{\text{eff}}(\theta) I_0 L, \tag{9}$$

where I_0 represents the intensity of the incident field, L represents the length of the thin sample, and k is the wave number in a vacuum. When the optical field propagates in a BaF_2 thick sample with the dimensionless normalized length M, the crystal can be seen as a collection of N thin samples, each of which has a dimensionless normalized length $\Delta\zeta = M/N$. Therefore, the nonlinear refractive phase shift when the optical field passes through the Nth thin sample can be expressed as

$$\delta_N = k n_{\text{eff}}(\theta) I_{N-1} \Delta\zeta, \tag{10}$$

where I_{N-1} represents the light intensity after passing through the $(N-1)$th thin sample. Eventually, the nonlinear refractive phase shifts created by the optical field whilst passing through each thin sample are combined to determine the total nonlinear refractive phase shift.

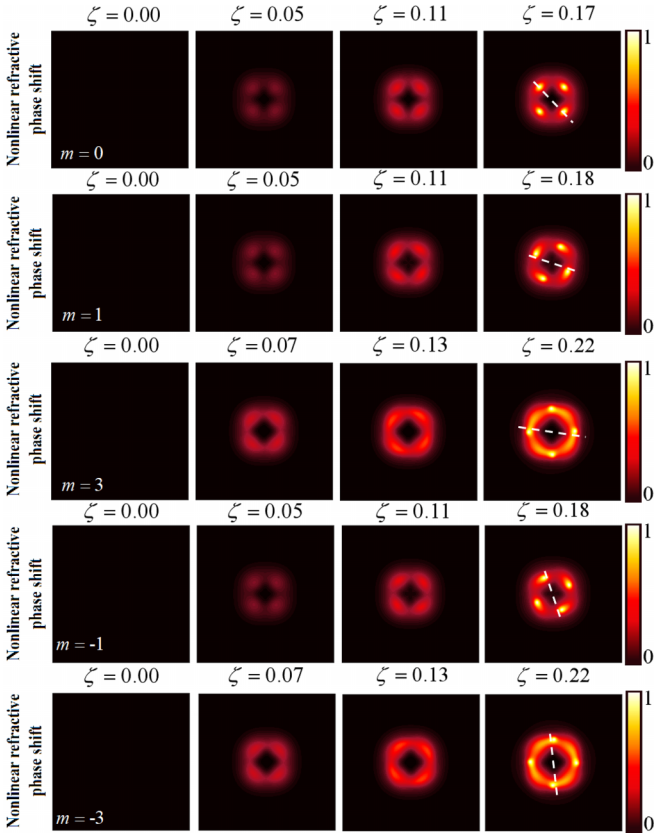

FIG. 7. The nonlinear refractive phase shift distribution of radially polarized vortex beams with different vortex phases propagating in a BaF_2 crystal. The topological charges of the vortex phases are $m = 0$ (first row), $m = \pm 1$ (second and fourth rows), and $m = \pm 3$ (third and fifth rows). Each row from left to right corresponds to four sequentially increasing propagation distances ζ. The white dotted lines reflect the change in rotation angle. The nonlinear refractive phase shift is normalized to its maximum value in each row separately. The color bar represents normalized nonlinear refractive phase shift values.

We simulated the variation of the nonlinear refractive phase shift distribution of a radially polarized vortex beam as it propagates through the BaF_2 crystal by means of Eq. (10), as shown in Fig. 7. When $m = 0$, as the propagation distance increases, the nonlinear refractive phase shift distribution will gradually concentrate on the four collapsed positions of the optical field, as shown in Fig. 7 (first row). When $m \neq 0$, as the propagation distance increases, the nonlinear refractive phase shift distribution not only gradually concentrates on the four collapsed positions of the optical field but also rotates, as shown in Fig. 7 (from the second row to the fifth row). If $m > 0$, the nonlinear refractive phase shift distribution rotates counterclockwise, as shown in Fig. 7 (second and third rows). If $m < 0$, the nonlinear refractive phase shift distribution rotates clockwise, as shown in Fig. 7 (fourth and fifth rows). For $m = \pm 1$, the nonlinear refractive phase shift distribution rotates by 20° during the whole collapse process, as shown in Fig. 7 (second and fourth rows). For $m = \pm 3$, the nonlinear refractive phase shift distribution rotates by 48° during the whole collapse process, as shown in Fig. 7 (third and fifth rows). The rotation angle during the propagation increases as the propagation distance and the absolute value of m increases. It can be clearly seen that the change in the nonlinear refractive phase shift distribution during the collapse is basically consistent with the change in phase and intensity. Thus, the reason for the rotation of the phase during collapse is explained.

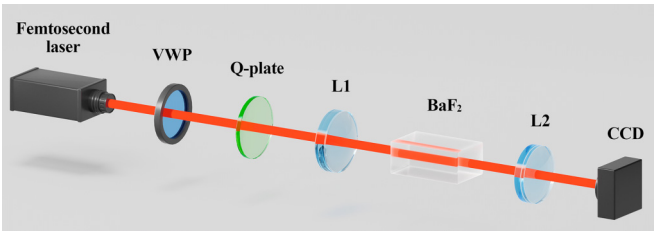

FIG. 8. The experimental prototype of radially polarized vortex beams propagating in a BaF_2 crystal. The laser is an 800-nm femtosecond laser. VWP is a first-order vortex wave plate. L1 is a focusing lens. L2 is an achromatic lens.

To sum up, due to the nonlinear interaction of the radially polarized vortex beam with the BaF_2 crystal, the optical field undergoes a kind of rotational nonlinear refractive phase shift during collapse. This phenomena affects the phase during propagation, causing a phase rotation in the optical field. Ultimately, the rotating phase leads to the rotation of the optical field during the collapse. This phase rotation is a special Gouy phase shift. It comes from the nonlinear interaction between the vector vortex beam and the anisotropic Kerr medium. Therefore, we consider the phase rotation of radially polarized vortex beams in BaF_2 crystals to be a nonlinearity-related Gouy phase shift.

To facilitate the realization of such a controllable helical collapse, we propose an experimental prototype, as shown in Fig. 8. The experiment can be composed of three critical sections: generation of radially polarized vortex beams, optical field collapse filamention in the medium, and detection of helical collapse filamention. Initially, we make the horizontal linearly polarized beam output from the 800-nm femtosecond laser pass through a first-order vortex wave plate and a q-plate successively. This process enables the generation of a radially polarized vortex beam. In the second step, the generated radially polarized vortex beam is passed through a focusing lens and positively incident along the [001] axis onto a 20-mm-long BaF_2 crystal. When the laser output power is greater than the critical power, this optical field will collapse into filaments in the crystal. Finally, the optical intensity pattern emitted from the BaF_2 crystal is collected by an achromatic lens and imaged onto a high-resolution CCD. The device can adjust the vortex phase of the radially polarized vortex beams by selecting q-plates with different parameters and thus observe the helical collapse in the BaF_2 crystal. In order to observe this nonlinearity-related Gouy phase shift more intuitively, an interferometer can be used to measure the wave-front phase of the beam before and after the filamentation.

V. CONCLUSIONS

In summary, this work presents a technique to rotate a radially polarized beam as it collapses into stable multifilament in a BaF_2 crystal by attaching a vortex phase to it. We

find a nonlinearity-related Gouy phase shift caused by the nonlinear interaction between the vector vortex beams and the anisotropic Kerr medium. It is shown that the nonlinear interaction between this optical field and the medium causes the spin-orbit coupling and produces a rotational nonlinear refractive phase shift. This rotational nonlinear refractive phase shift affects the phase during the collapse, leading to a nonlinearity-related Gouy phase shift. Finally, the phase rotation prompts the rotation of the optical field. The rotation of the optical field is determined by the OAM carried by the incident field. The direction and angle of the rotation during collapse can be controlled by adjusting the vortex potential phase topological charge. In addition, we give a prototypical experimental paradigm regarding the controllable helical collapse of optical fields. This approach and its physical mechanism provide new perspectives and methods for controlling optical field collapse filamentation and have potential applications in many fields.

ACKNOWLEDGMENTS

We acknowledge support from the National Natural Science Foundation of China (Grants No. 12104333, No. 52106024, and No. 11974258).

[1] L. Xu, D. Li, J. Chang, T. Xi, and Z. Hao, Results Phys. **26**, 104334 (2021).
[2] N. Barbieri, Z. Hosseinimakarem, K. Lim, M. Durand, M. Baudelet, E. Johnson, and M. Richardson, Appl. Phys. Lett. **104**, 261109 (2014).
[3] J.-Q. Lü, P.-P. Li, D. Wang, C. Tu, Y. Li, and H.-T. Wang, Opt. Express **26**, 29527 (2018).
[4] P. Robinson, Rev. Mod. Phys. **69**, 507 (1997).
[5] L. Bergé, Phys. Rep. **303**, 259 (1998).
[6] G. Fibich and B. Ilan, Physica D (Amsterdam, Neth.) **157**, 112 (2001).
[7] A. Couairon and A. Mysyrowicz, Phys. Rep. **441**, 47 (2007).
[8] L. Bergé, S. Skupin, R. Nuter, J. Kasparian, and J.-P. Wolf, Rep. Prog. Phys. **70**, 1633 (2007).
[9] S. A. Akhmanov, A. P. Sukhorukov, and R. V. Khokhlov, Sov. Phys. JETP **23**, 1025 (1966).
[10] J. M. Soto-Crespo, E. M. Wright, and N. N. Akhmediev, Phys. Rev. A **45**, 3168 (1992).
[11] L. Bergé, C. Gouédard, J. Schjødt-Eriksen, and H. Ward, Physica D (Amsterdam, Neth.) **176**, 181 (2003).
[12] A. Vinçotte and L. Bergé, Physica D (Amsterdam, Neth.) **223**, 163 (2006).
[13] A. Dubietis, G. Tamosauskas, G. Fibich, and B. Ilan, Opt. Lett. **29**, 1126 (2004).
[14] T. D. Grow and A. L. Gaeta, Opt. Express **13**, 4594 (2005).
[15] T. Pfeifer, L. Gallmann, M. J. Abel, D. M. Neumark, and S. R. Leone, Opt. Lett. **31**, 2326 (2006).
[16] D. Li, T. Xi, L. Zhang, H. Tao, X. Gao, J. Lin, and Z. Hao, Opt. Express **25**, 23910 (2017).
[17] Z. Hao, K. Stelmaszczyk, P. Rohwetter, W. M. Nakaema, and L. Woeste, Opt. Express **19**, 7799 (2011).
[18] V. Kandidov, N. Akozbek, M. Scalora, O. Kosareva, A. Nyakk, Q. Luo, S. Hosseini, and S. Chin, Appl. Phys. B **80**, 267 (2005).
[19] S.-M. Li, Y. Li, X.-L. Wang, L.-J. Kong, K. Lou, C. Tu, Y. Tian, and H.-T. Wang, Sci. Rep. **2**, 1007 (2012).
[20] S.-M. Li, Z.-C. Ren, L.-J. Kong, S.-X. Qian, C. Tu, Y. Li, and H.-T. Wang, Photonics Res. **4**, B29 (2016).
[21] D. Wang, G.-G. Liu, J.-Q. Lü, P.-P. Li, M.-Q. Cai, G.-L. Zhang, Y. Li, C. Tu, and H.-T. Wang, Opt. Express **26**, 27726 (2018).
[22] L. Lu, Z. Wang, and Y. Cai, Opt. Express **30**, 15905 (2022).
[23] D. Wang, Y. Pan, J.-Q. Lü, P.-P. Li, G.-G. Liu, M.-Q. Cai, Y. Li, C. Tu, and H.-T. Wang, J. Opt. Soc. Am. B **35**, 2373 (2018).
[24] D. Wang, R.-W. Li, X. Zhang, F. Feng, H. Feng, L. Lu, B. Feng, S.-D. Liu, and Z.-Q. Nie, Opt. Express **32**, 5230 (2024).
[25] L. T. Vuong, T. D. Grow, A. Ishaaya, A. L. Gaeta, G. W. 't Hooft, E. R. Eliel, and G. Fibich, Phys. Rev. Lett. **96**, 133901 (2006).
[26] V. Jukna, C. Milián, C. Xie, T. Itina, J. Dudley, F. Courvoisier, and A. Couairon, Opt. Express **22**, 25410 (2014).
[27] P. Polynkin, C. Ament, and J. V. Moloney, Phys. Rev. Lett. **111**, 023901 (2013).
[28] Y. Ren, M. Alshershby, Z. Hao, Z. Zhao, and J. Lin, Phys. Rev. E **88**, 013104 (2013).
[29] A. Camino, Z. Hao, X. Liu, and J. Lin, Opt. Lett. **39**, 747 (2014).
[30] B. Yan, H. Liu, C. Li, X. Jiang, X. Li, J. Hou, H. Zhang, W. Lin, B. Liu, and J. Liu, Opt. Laser Technol. **131**, 106391 (2020).
[31] J. Zhao, L. Guo, W. Chu, B. Zeng, H. Gao, Y. Cheng, and W. Liu, Opt. Lett. **40**, 3838 (2015).
[32] G. Fibich and A. L. Gaeta, Opt. Lett. **25**, 335 (2000).
[33] A. Jullien, O. Albert, G. Chériaux, J. Etchepare, S. Kourtev, N. Minkovski, and S. M. Saltiel, J. Opt. Soc. Am. B **22**, 2635 (2005).
[34] K. Kawano and T. Kitoh, *Introduction to Optical Waveguide Analysis: Solving Maxwell's Equation and the Schrödinger Equation* (Wiley & Sons, New York, 2001).
[35] L. Allen, M. W. Beijersbergen, R. J. C. Spreeuw, and J. P. Woerdman, Phys. Rev. A **45**, 8185 (1992).
[36] S. M. Barnett, M. Babiker, and M. J. Padgett, Phil. Trans. R. Soc. A **375**, 20150444 (2017).
[37] K. Y. Bliokh, A. Y. Bekshaev, and F. Nori, Nat. Commun. **5**, 3300 (2014).
[38] S. M. Barnett, J. Opt. B: Quantum Semiclassical Opt. **4**, S7 (2001).
[39] S. Fu, C. Guo, G. Liu, Y. Li, H. Yin, Z. Li, and Z. Chen, Phys. Rev. Lett. **123**, 243904 (2019).
[40] Y. Zhang, Z. Zhang, H. Lin, Z. Nie, R. Feng, Y. Zhao, and B. Jia, Light: Adv. Manuf. **4**, 348 (2023).
[41] K. Y. Bliokh, F. J. Rodríguez-Fortuño, F. Nori, and A. V. Zayats, Nat. Photonics **9**, 796 (2015).
[42] L. Marrucci, C. Manzo, and D. Paparo, Phys. Rev. Lett. **96**, 163905 (2006).
[43] S. Feng and H. G. Winful, Opt. Lett. **26**, 485 (2001).

[44] M. W. Beijersbergen, L. Allen, H. Van der Veen, and J. Woerdman, Opt. Commun. **96**, 123 (1993).

[45] K. J. Kaltenecker, J. C. König-Otto, M. Mittendorff, S. Winnerl, H. Schneider, M. Helm, H. Helm, M. Walther, and B. M. Fischer, Optica **3**, 35 (2016).

[46] Y. Zhang, X. Liu, H. Lin, D. Wang, E. Cao, S. Liu, Z. Nie, and B. Jia, Opto-Electron. Adv. **5**, 210026 (2022).

[47] Z.-Q. Nie, H. Lin, X.-F. Liu, A.-P. Zhai, Y.-T. Tian, W.-J. Wang, D.-Y. Li, W.-Q. Ding, X.-R. Zhang, Y.-L. Song *et al.*, Light: Sci. Appl. **6**, e17032 (2017).

[48] B. Gu, B. Wen, G. Rui, Y. Xue, Q. Zhan, and Y. Cui, Opt. Lett. **41**, 1566 (2016).

[49] R. DeSalvo, M. Sheik-Bahae, A. Said, D. J. Hagan, and E. W. Van Stryland, Opt. Lett. **18**, 194 (1993).